ENVIRONMENTAL RESEARCH
LETTERS

LETTER • OPEN ACCESS

Observational evidence of intensified nocturnal urban heat island during heatwaves in European cities

ENVIRONMENTAL RESEARCH
LETTERS

LETTER

Observational evidence of intensified nocturnal urban heat island during heatwaves in European cities

Marco Possega*, Leonardo Aragão, Paolo Ruggieri, Marco Antonio Santo[1] and Silvana Di Sabatino

Department of Physics and Astronomy, University of Bologna, Bologna, Italy
[1] Current address: ARPAE, Emilia Romagna Regional Agency for Prevention, Environment and Energy, Bologna, Italy
* Author to whom any correspondence should be addressed.

E-mail: marco.possega2@unibo.it

Keywords: heatwave, urban heat island, urban climate, European cities

Supplementary material for this article is available online

OPEN ACCESS

RECEIVED
25 July 2022

REVISED
7 November 2022

ACCEPTED FOR PUBLICATION
17 November 2022

PUBLISHED
25 November 2022

Abstract

A heatwave (HW) is a large-scale meteorological event characterised by persistent and extremely high-temperature condition. At the local scale, the urban heat island (UHI) is another thermal-related phenomenon defined as an urban area warmer than its surrounding regions due to different surfaces' capabilities to absorb and store heat. However, the assessment about the effect produced on UHI by HW events is not homogeneous. Indeed, regarding the capability of HWs to influence the urban-rural temperature difference, several studies report different conclusions describing both an exacerbation and a reduction of UHI during HW events. In this context, the present study analyses *in situ* long records of temperature measurements (20 years) to provide observational shreds of evidence of UHI modification under HW conditions. We examine data from the European Climate Assessment & Dataset and World Meteorological Organization computing the UHI index (UHII) to quantify the UHI effect intensity in 37 European cities during the last 20 summers. The results show an UHII intensification for 28 of the 32 cities affected by positive UHI during extremely high temperatures at night, while substantial variations are not observed during the daytime. The time evolution of UHI during a HW highlights that a more significant and persistent urban-rural temperature gradient explains the UHI intensification. Finally, the relationship between the large and local-scale temperature phenomena reveals that continental high-temperature periods are often associated with prominent temperature differences between small-scale urban and rural environments, assessing the impact of large-scale features on thermal stress at the local scale.

1. Introduction

A heatwave (HW) is a meteorological phenomenon that features large-scale persistent high-temperature conditions and can severely affect urban and rural environments. Two examples of impactful episodes experienced by the European continent are the 2003 Central Europe HW, characterised by reiterated temperatures of 35 °C to 40 °C which caused economic damages superior to 13 billion euros [1] and more than 70 000 life losses [2], and the 2010 Eastern Europe/Russia HW, that provoked more than 50 000 deaths in several countries [3]. The Sixth Assessment Report of the IPCC [4] stated that it is *virtually certain* that HWs have become more frequent and intense since the 1950 s, and this trend will continue in the following decades due to climate change [5–7].

At the local scale, urban areas can be subject to another heat-related phenomenon termed urban heat island (UHI), defined as a significant temperature difference between urban and surroundings environments [8], with generally higher temperature differences at night than during the day for a more stable atmosphere. According to [9], UHIs originate from differences in urban and rural cooling and

warming rates due to numerous factors as radiation, sensible/latent heat fluxes, advection and anthropogenic sources [10]. For example, while in rural areas the vegetation cools down the air by transpiring water from plant leaves, the urban buildings restrain wind flows and traps the release of radiative solar energy. Consequently, the urban surface stores heat and establishes a positive urban–rural temperature gradient ΔT, especially three to five hours after sunset when rural areas cool off faster than urban.

The occurrence of HW can significantly modify UHI characteristics, considering that clear sky condition promotes an increment in incoming shortwave radiation, the high temperature reaching the upper levels inhibits the advective cooling effect, and the released anthropogenic heat increases due to higher air conditioners demand [11]. It is therefore reasonable to expect an UHI magnitude intensification concurrently with HW events. At the same time, the possibility of HW-drought co-occurrence [12] must be taken into account, possibly generating more severe impacts than the occurrence of individual extremes especially on water scarcity in soils [13]. Indeed, poor rainfall produces a diminution in soil wetness, reducing the evapotranspiration cooling effect in rural areas whereas the impact on urban temperature is minimum [14], and UHI can undergo a decrease during HWs [15].

Numerous studies examined the interaction between these two different scale phenomena following various approaches. Employing numerical simulations, many studies assessed the existence of a synergistic behaviour producing intensified urban–rural temperature differences in HW conditions especially in US locations [16, 17], also suggesting that added heat stress in cities is higher than the sum of the background UHI and the HW effect [18]. Conversely, other numerical studies such as [19] retrieved the absence of significant HW-UHI synergistic interaction, even for the USA [20].

Besides the modelling approach, also observational studies addressing different locations and HW events examined the UHI-HW interaction. For example, [21] retrieved an UHI increment in Madison, USA, during summertime HWs and the same is found for the metropolitan city of Karachi, Pakistan [22], for Beijing [23] and for Athens [24] especially during nighttime. A study regarding Shanghai [25] evidenced an UHI amplification during HW depending on localized effects, retrieving that less urbanized districts were generally more sensitive to this synergy. Also different rural backgrounds are proven to be crucial in determining the HW-induced UHI augmentation, particularly the rural evapotranspiration cooling effects based on humidity and vegetation type [26]. On the other hand, in [14] and [27] observational and reanalysis data were used to analyse UHI intensity during hot temperature extremes in France and in Portugal, and did not find significant UHI-HW interactions.

Along these lines, [28] currently reviewed the scientific literature on UHI-HW interaction concluding that most examined studies indicate an UHI increase during HWs, although others detect no significant synergy or even a reduction of UHI intensity during HWs. However, the lack of widely accepted multi-scale modelling approaches and inhomogeneities in data and methodologies adopted blur the picture on UHI-HW interaction and raise questions on its robustness. In [28] several research gaps highlight the necessity to investigate multi-year datasets instead of single HW events and the importance of considering an ensemble of cities with different characteristics to reveal the large-scale general trend. The present study attempts to fill these gaps for the European continent, refining the methodology used by [29] which investigated a large ensemble of USA cities through *in situ* meteorological records and observed a reduced UHI intensity during warmer synoptic conditions, a result remarkably in contrast with the majority of studies. Bearing also in mind the different morphology of European and USA cities [30], it is therefore unclear whether European cities behave like those examined by [29] or they follow the dominant paradigm of positive UHI-HW correlation. Our approach can help clarify this question and can complement existing literature on specific case studies for European cities (e.g. [31–33]) by providing an unprecedented assessment through observational data for Europe about impacts of large-scale features on thermal stress at local scale. In particular, we evaluate the HW effects on UHI in 37 European cities over a period of 20 years with an empirical approach, estimating UHI intensity from daily minimum/maximum temperature measured by stations. We focus particularly on summer nighttime, when UHI effect is generally more pronounced and dangerous for human health [34].

Section 2 contains the description of the datasets employed, definitions and analysis methods. Section 3 presents the results about the UHI-HW relationship. Section 4 provides a concluding discussion of the study and suggestions for future developments.

2. Data and methods

2.1. Data sources

In this study we examined the temperatures of European urban and surrounding areas employing stations data gathered by European Climate Assessment & Dataset (ECA&D [35] and [36]) and by World Meteorological Organization network (WMO [37]), provided by NOAA's National Centers for Environmental Information (NCEI). The analysis covered 20 years (2000–2019) of boreal summers (June, July and August), following recommendations of [38] and

Table 1. Cities analysed with the coordinates of the city centres. *Source*: Wolfram Knowledgebase™ [47].

List of selected locations					
Location	Latitude	Longitude	Location	Latitude	Longitude
1) Aachen	50.77 N	6.09 E	20) Karlsruhe	49.00 N	8.04 E
2) Amsterdam	52.37 N	4.89 E	21) Leipzig	51.35 N	12.40 E
3) Antwerp	51.22 N	4.42 E	22) Lisbon	38.72 N	9.14 W
4) Athens	37.98 N	23.73 E	23) Ljubljana	46.06 N	14.51 E
5) Berlin	52.52 N	13.38 E	24) London	51.50 N	0.12 W
6) Bologna	44.50 N	11.34 E	25) Madrid	40.42 N	3.71 W
7) Bremen	53.08 N	8.81 E	26) Malmo	55.61 N	13.02 E
8) Brussels	50.83 N	4.33 E	27) Mannheim	49.50 N	8.47 E
9) Budapest	47.51 N	19.08 E	28) Munich	48.14 N	11.58 E
10) Catania	37.50 N	15.08 E	29) Nuremberg	49.45 N	11.05 E
11) Cologne	50.95 N	6.97 E	30) Paris	48.86 N	2.34 E
12) Copenhagen	55.68 N	12.57 E	31) Saarbrucken	49.25 N	6.97 E
13) Dresden	51.05 N	13.74 E	32) Stockholm	59.33 N	18.07 E
14) Dublin	53.33 N	6.25 W	33) Stuttgart	48.79 N	9.19 E
15) Frankfurt	50.12 N	8.68 E	34) Toulouse	43.62 N	1.45 E
16) Goteborg	57.72 N	12.01 E	35) Vienna	48.22 N	16.37 E
17) Hamburg	53.55 N	10.00 E	36) Zagreb	45.80 N	15.97 E
18) Hanover	52.40 N	9.73 E	37) Zurich	47.38 N	8.54 E
19) Helsinki	60.17 N	24.94 E			

[39]. Additionally, to select the appropriate stations for UHI analysis we took advantage of the urban climate dataset provided by Copernicus Climate Change Service (C3S [40]) and of land cover characteristics furnished by CORINE Land Cover 2018 inventory (CLC [41]). For HW identification we used the ECMWF Reanalysis 5th Generation (ERA5) dataset [42], which provides hourly data on atmospheric, land-surface and sea-state parameters on regular latitude–longitude grids at $0.25° \times 0.25°$ resolution. Since the purpose was to detect large scale HW phenomena, ERA5 dataset was chosen as in [43], also due to its documented applicability for developing heat-related quality-checked products (see [44, 45]).

2.2. Method to select cities and weather stations

The selection of weather stations started from European cities having more than 150 000 inhabitants [46] and with available temperature data in ECA&D or WMO repositories. We employed three parameters to ensure the uniformity of the analysis and to reduce the heterogeneity of dataset characteristics:

(a) The maximum distance of urban and rural stations from the central point of the city (according to the coordinates provided by [47] and reported in table 1), necessary to guarantee a homogeneous analysis among cities with different sizes. We considered urban stations within a distance $D \leqslant 10$ km from the city centre, a choice supported by checking the European Urban Atlas [48] which suggested this value as the average radius of the urban area for analysed cities. Rural stations were selected at a distance $10 < D \leqslant 35$ km from the city centre, with an additional check on stations positioned near 10 km to distinguish urban from rural ones. The 35 km threshold fits in the range between one and 50 km identified by [49], which reviewed studies about effects of rural extent on UHI. This adopted parameter was similar to [29] to have a solid reference and to enable comparisons with another study focusing on highly populated cities through observational data. Other thresholds like 20 km as in [50] were tested for rural distance, obtaining unaltered results;

(b) the maximum height difference between urban and rural stations, necessary to remove the impact of topography on UHI evaluation. The average altitude difference between urban and rural stations ΔH was established to be smaller than ± 70 m. This threshold differs from the ± 30 m indicated by [51] to increase the number of stations included and the analysis strength. We also performed sensitivity tests using ± 30 m without noticing significant variations in the results;

(c) a check of land cover like in [29], since [52] recommends to select rural areas in terrains surrounded by natural properties, without densely constructed buildings. We imposed that urban stations must present land cover characteristics of urban areas according to the rural–urban mask of C3S based on CLC inventory, also discussed in [53]. The CLC's method classifies each pixel obtained on satellite images into different land cover classes, as described in [54]. Although C3S does not provide this mask for all the cities analysed, we were able to reproduce it for the missing locations following the C3S method,

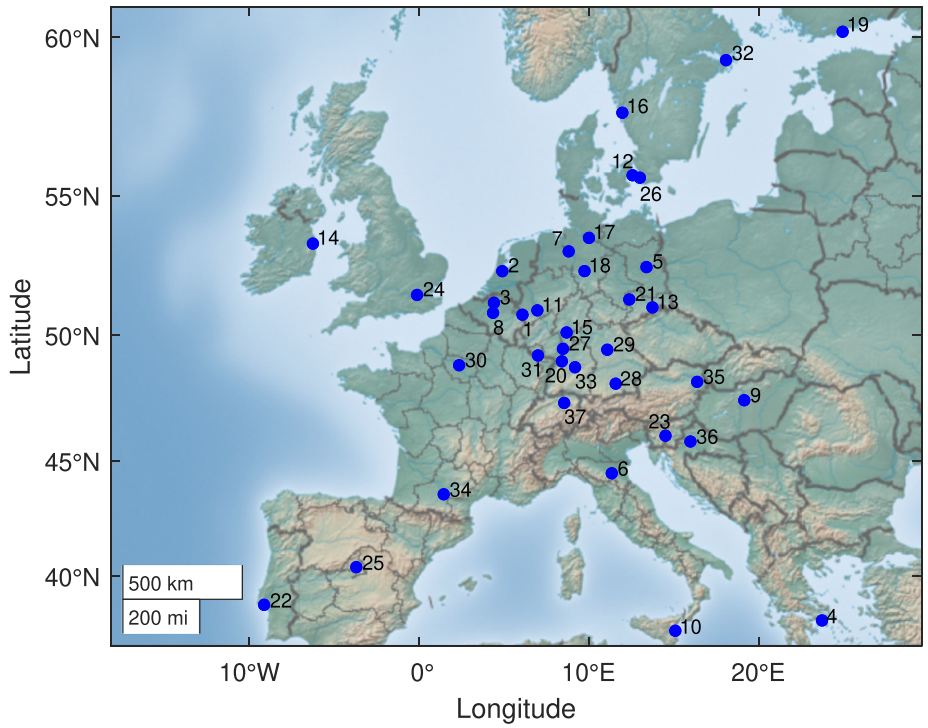

Figure 1. Geographical distribution over the European continent of the cities composing the final dataset. The numbers refer to locations reported in table 1.

which does not distinguish urban from suburban areas and considers no urban zones as rural.

2.3. Selection results

Following the described methodology we were able to identify 37 cities. The geographical distribution of these cities (figure 1) covers areas with different geographical features of the European continent such as latitude, distance from the sea and altitude.

Figure 2(left) shows the percentage of stations located at different distances from the city centres, where more than 80% of the stations are placed at a distance $D \leqslant 8$ km from the city centre. Rural sites exhibit a homogeneous distribution from $15 \leqslant D \leqslant 35$ km, while only a small percentage positioned between 9 and 15 km (figures S1 and S2 in the supplementary material display the location of each station). Figure 2(right) contains the histogram of rural stations settled at various height difference $|\Delta H|$ from the city centre and shows more than 50% of the stations attending the $|\Delta H| \leqslant 30$ m [51], while the more $|\Delta H|$ increases, the less the number of stations. Despite the abundance of rural stations with $|\Delta H| > 30$ m, we considered that the temperature difference produced did not significantly affect our analysis which regarded the differences during HW and NO days, when this altitude effect acts likewise.

2.4. Method for heatwaves identification

To identify HWs we reproduced the methodology of [39], based on gridded and multi-year datasets and applied specifically to the European continent. For each ERA5 gridpoint we evaluated daily temperature anomalies with respect to the 2000–2019 climatology extracted from the ERA5 dataset. We identified extremely hot days when anomalies exceeded the upper 95th percentile (T_{95}) of the local probability density function, computed for each day d using the 21 d centred moving average ($d-10$ and $d+10$) along the 20 summers of temperature data. We selected each city reference gridpoint nearest to the coordinates shown in table 1. To take into account the spatial extension of HWs and to avoid considering isolated hot gridpoints, we required that T_{95} threshold had to be overcome in at least 60% of a square of side $L = 1°$, namely a 5×5 gridpoints matrix centred on the city reference gridpoint. If these two criteria were satisfied for at least three consecutive days, we labelled all days in this time interval as HW days. All days not considered HW days were defined normal summer days (NO) as in [38]. To verify the reliability of the results, we examined other HW definitions involving different thresholds. In particular, we tested the definition based on the temperature 90th percentile for three days persistence applied by [55], and the definition used by [56], shifting the temporal threshold to four days.

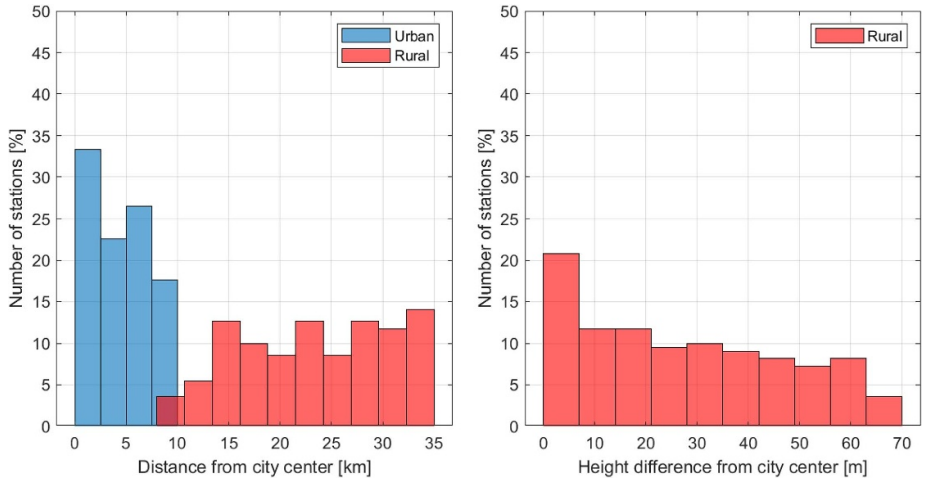

Figure 2. Characteristics of meteorological stations employed: on the left histogram of the distance D from city centres of urban (cyan) and rural (red) stations; on the right histogram of the height difference $|\Delta H|$ from the city centres of rural stations.

2.5. UHI Index

We determined for each city the daily intensity of UHI effect by calculating a Composite UHI index (UHII) as defined in [57] and [58]:

$$UHII = \overline{T_U} - \overline{T_R}, \tag{1}$$

where T_U and T_R are the urban and rural temperatures, respectively, and the overline indicates that values are averaged over all the employed stations. Compared to the original definition based on a couple of observations [59], this UHII was chosen since it allows to reduce the impact of site-specific variability.

2.6. Methods of temperature-related analysis

The first part of the analysis investigated the different behaviour of the UHI index during HW and NO conditions from a statistical perspective, by comparing the mean UHII during HWs ($\overline{UHII}_{\mathrm{HW}}$) to the mean UHII during NO days ($\overline{UHII}_{\mathrm{NO}}$), calculating separately the case for nocturnal and for diurnal values. The results for daytime exhibited negligible variations of UHII during HWs, while considerable modifications were retrieved for nighttime UHII, so a detailed analysis was focused on nocturnal UHII. We performed a Welch t-test [60], reliable for two unequal sample sizes [61], to reject the null hypothesis that the two samples belonged to the same distribution. To compute the t value, we employed the effective sample size estimated as in [62]. To retrieve the potential effects of intra-seasonality for each city, the intra-seasonal cycle of UHII for each day was calculated and averaged over the 20 years of data, and compared with the UHII daily anomaly computed respecting this intra-seasonal cycle. We also investigated the frequency of positive UHII days during NO and HW, and we explored the Pearson correlation among UHII and some cities' characteristics.

The second part concerned the UHII temporal evolution during HW occurrences, also in relation to the behaviour of large scale temperature anomaly T_{AN} with respect to computed T_{95}. The aim was to analyse HW impacts on UHI more precisely with respect to the statistical investigation, observing shapes and shifts of the signals. We standardised both UHII and T_{AN} by their climatological values (2000–2019). In particular, urban and rural temperature data (and their ΔT) relative to the same lag day i with respect to HW onset were averaged over the number of HWs for each city, obtaining a mean value T_i. Then, we standardised these mean values to scale the UHI modifications according to the different city features. The standardised temperature $\widetilde{T}_i$ referring to lag day i was calculated for every city as

$$\widetilde{T}_i = \frac{T_i - \overline{T}}{\sigma_{T_i}}, \tag{2}$$

where σ_{T_i} is the T_i relative standard deviation, and $\overline{T}$ is the 20 years climatological value, including both HW and NO days. To identify possible temperature spikes, we determined the temperature values of each HW day d calculating the moving average of the interval between $d - n \cdot r_{\mathrm{HW}}$ and $d + n \cdot r_{\mathrm{HW}}$, where r_{HW} is the HW duration and n is an integer set equal to 1,2 or 3, and then we compared the results to those previously obtained. Finally, we evaluated the correlation between UHI and T_{AN} intensities.

3. Results and discussion

3.1. Characteristics of identified heatwaves

The methodology presented in section 2.4 identified from 1 to 10 HW events for each city (table 2). Figure 3 shows the geographical distribution of HW properties across the European cities, highlighting the average HW duration and the average HW intensity.

Table 2. Number of detected HWs for each location.

Location	Number of HWs	Location	Number of HWs
1) Aachen	7	20) Karlsruhe	7
2) Amsterdam	5	21) Leipzig	4
3) Antwerp	9	22) Lisbon	2
4) Athens	1	23) Ljubljana	5
5) Berlin	5	24) London	6
6) Bologna	3	25) Madrid	9
7) Bremen	7	26) Malmo	2
8) Brussels	10	27) Mannheim	6
9) Budapest	10	28) Munich	7
10) Catania	3	29) Nuremberg	8
11) Cologne	7	30) Paris	6
12) Copenhagen	3	31) Saarbrucken	6
13) Dresden	6	32) Stockholm	5
14) Dublin	2	33) Stuttgart	5
15) Frankfurt	7	34) Toulouse	4
16) Goteborg	3	35) Vienna	8
17) Hamburg	6	36) Zagreb	6
18) Hanover	7	37) Zurich	6
19) Helsinki	1		

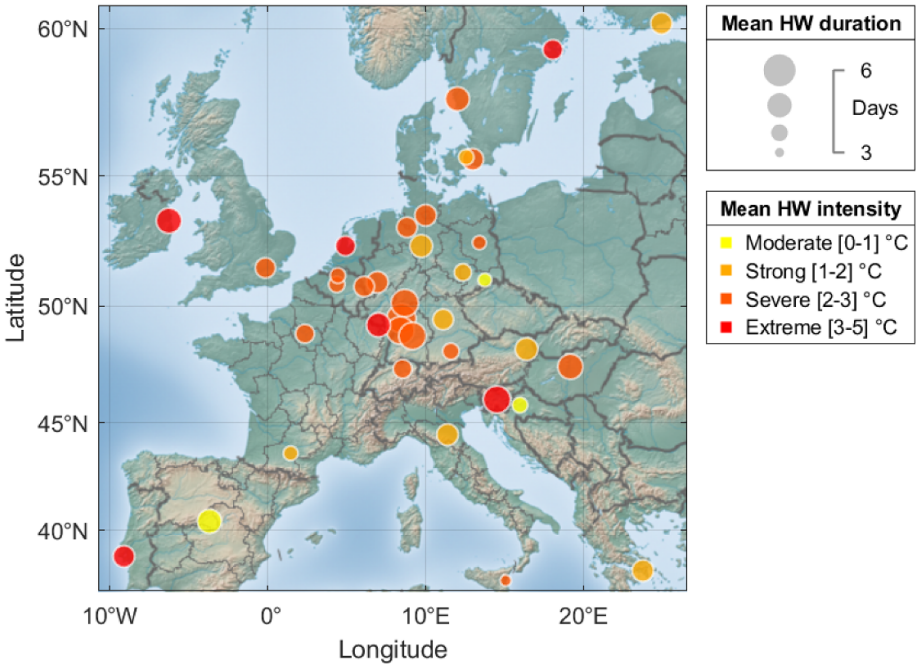

Figure 3. Geographic distribution of heatwave features for analysed cities: the dot size indicates the average duration [days] of HWs detected, while the colour depicts the average HW intensity.

The latter describes the mean large scale temperature anomaly $\overline{T_{AN}}$ during HW events. The average HW duration for the 37 cities varies between three and six days, but for 28/37 cities it does not exceed four days. The HW intensity classification presented in figure 3, often employed in marine HW studies [63], shows that 27% and 51% of cities experienced strong and severe intensity events since 2000, respectively.

3.2. Analysis of the UHI-HW relationship

We analysed the behaviour of UHI during NO days and HW days for the 37 selected cities. The results for daytime UHI revealed negligible variations of UHII during HWs, while substantial modifications were observed for nighttime, regarding which we addressed the in-depth analysis. Figure 4(a) shows nocturnal $\overline{UHII}_{NO}$ and $\overline{UHII}_{HW}$ values with the corresponding standard deviation for each city,

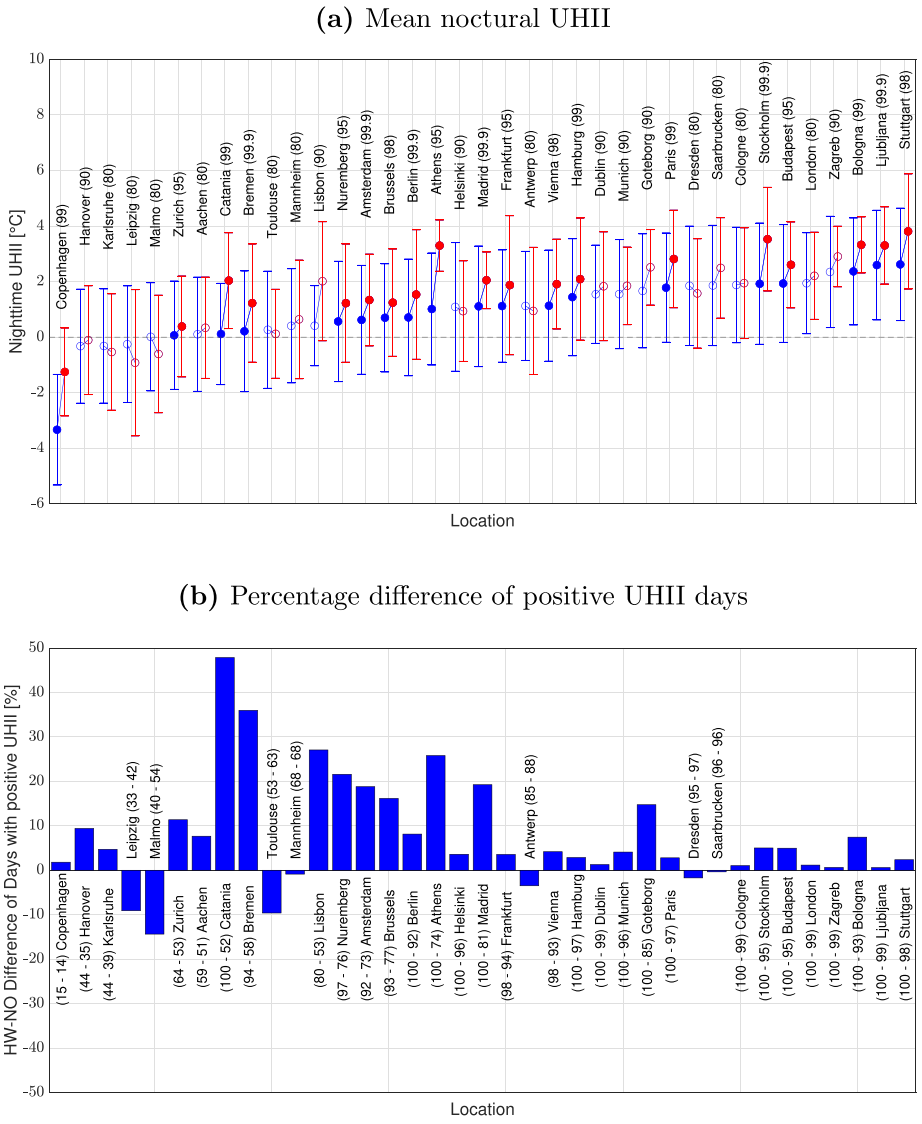

Figure 4. (a) Mean and standard deviation of nighttime UHII values, where for each analysed city the blue dot indicates $UHII_{NO}$ and the red dot is $UHII_{HW}$. The numbers between parentheses represent the statistical significance, and filled dots refer to results with significance $> 95\%$. (b) Difference between HW and NO of the percentage of days with positive UHII. The numbers between parenthesis are HW and NO percentages.

computed averaging respectively over NO and HW days for the 20 summers. The cities are sorted by the magnitude of $\overline{UHII}_{NO}$, where some of them presented negative values, indicating that the adopted methodology did not sample the UHI effect for a subset of cities. Excluding not statistically significant results, only Copenhagen exhibited $\overline{UHII} < 0$ values.

Focusing on the subset of 32 cities where a positive $\overline{UHII}_{NO}$ was retrieved, we see that for 28 out of 32 the $\overline{UHII}$ increases during HW days. The intensification is on average 0.7 °C (roughly 50% of the average magnitude of $\overline{UHII}_{NO}$). The Welch t-test revealed that 18 out of 28 cities presenting $\overline{UHII}$ increment provided statistically significant results with a confidence level $p = 0.05$, while 10/28 did not ($p \geqslant 0.2$). The test described in section 2.6 regarding the potential influence of intra-seasonality showed that $\overline{UHII}$ values did not depend on intra-seasonal variability. Indeed, the comparison between the intra-seasonal cycle daily anomaly of $\overline{UHII}$ with respect the $\overline{UHII}$ previously computed produced negligible variations.

To observe the impact of different HW definitions on presented results, we reproduced the analysis of figure 4(a) modifying the HW temperature and duration thresholds (as [55] and [56]). The outcomes showed slightly different values, but the behaviour was the same retrieved with the [39] methodology for all the cities with statistically significant results. Indeed, the obtained results confirmed the increment of nocturnal UHII for all significant locations with positive $\overline{UHII}_{NO}$.

Figure 4(b) shows the HW-NO percentage difference of days with positive UHII. Here, 25 out of the 32 cities with $\overline{UHII}_{NO} > 0$ exhibited an increase in percentage, and 18/25 were statistically significant. The amplification of $\overline{UHII}$ and percentage of days appeared slightly linearly correlated (Pearson correlation coefficient of about 0.5). This figure helps to

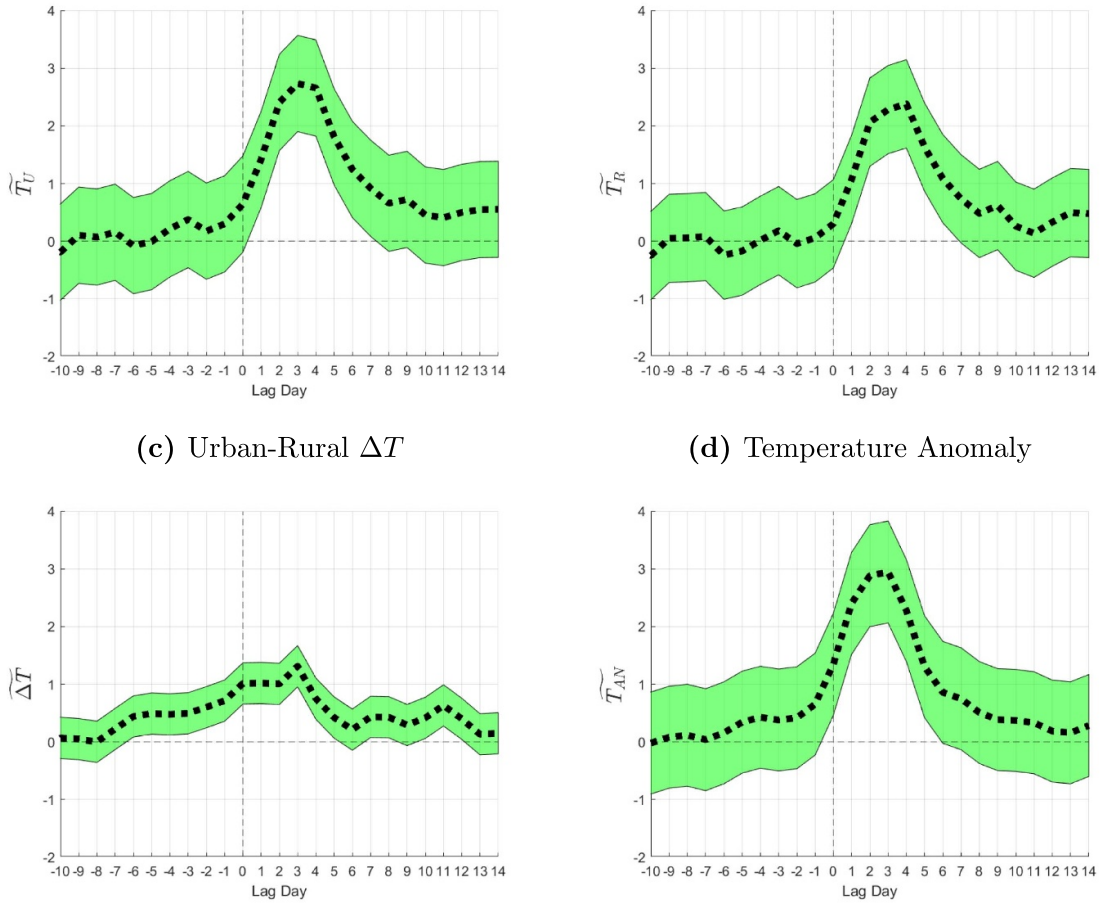

Figure 5. Temporal evolution during HW events averaged over the selected cities: (a) is the standardised urban temperature, (b) is the standardised rural temperature, (c) is the standardised urban–rural ΔT and (d) is the standardised large scale temperature anomaly with respect to T_{95}. The black dashed lines represent the mean value obtained averaging on cities which exhibit positive UHI effect, while the green area is the standard deviation.

understand the contribution of $UHII > 0$ frequency to the intensification during HWs. In particular, we distinguish three groups with different behaviours. The left side of the graph contains cities having $\overline{UHII}_{\mathrm{NO}}$ and irregular variations in the percentage. The central area includes (with few exceptions) locations exhibiting relatively small $\overline{UHII}_{\mathrm{NO}}$ values, but $UHII_{\mathrm{NO}} > 0$ percentage undergoing large increment for days with $UHII_{\mathrm{HW}} > 0$, meaning that UHI exacerbation was due to a higher frequency of positive UHI nights. The right side shows cities presenting high $\overline{UHII}_{\mathrm{NO}}$ values, and a $UHII_{\mathrm{NO}} > 0$ percentage near 100% which did not experience substantial modifications during HWs, so the primary cause of UHI exacerbation were larger UHII values, rather than higher frequency of $UHII > 0$ days.

We analysed the characteristics of cities and stations to detect common features between locations showing similar $\overline{UHII}$ behaviour. We evaluated linear correlations between UHII values and several variables, i.e. urban altitude, population, latitude, longitude, distance from the sea, urban-rural stations ΔH and urban-rural stations distance. Nonetheless, no significant correlations were retrieved (Pearson coefficient always smaller than $|0.36|$). Small correlation between UHII and urban–rural stations ΔH confirmed the possibility to extend the $\Delta H \leqslant 30$ m threshold proposed by [51] without noticeably affecting the analysis.

After the statistical $\overline{UHII}$ variations between NO and HW periods, we analysed the temporal evolution of nighttime temperatures and UHII during HW events. Figure 5 depicts the behaviour from 10 d before to 14 d after HW onset of urban and rural standardised temperature and their ΔT (representing the UHI), retrieved by averaging over the 32 cities with a positive $\overline{UHII}_{\mathrm{NO}}$. Both urban and rural temperature (figures 5(a) and (b)) show a symmetrical evolution, gradually increasing from day 0, reaching the peak around day 3–4 and then diminishing, but with significant differences. The most relevant is the discrepancy between the two maximum values of T_U and T_R, indicating that a few days after HW occurrence the urban temperature tended to amplify more than rural temperature, reaching higher absolute values. Observing the trend of the two curves before and

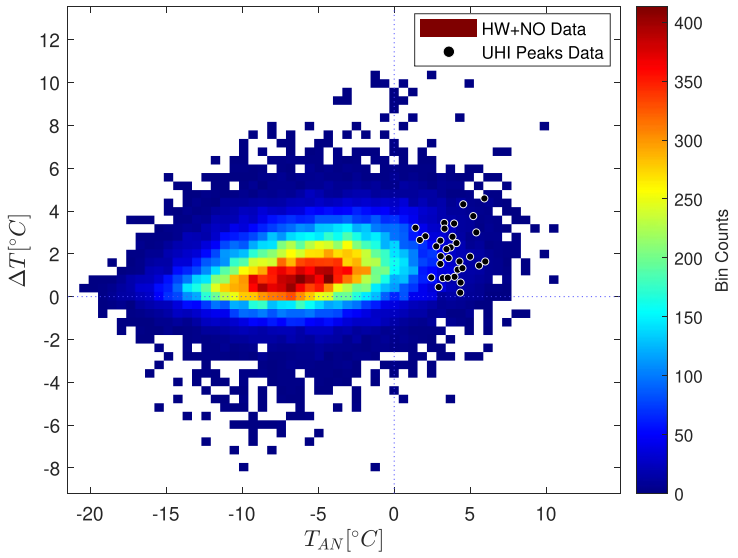

Figure 6. Binned scatter plot between large scale T_{AN} with respect to T_{95} and nocturnal urban-rural ΔT, including all data during both NO and HW days relative to 32 cities with $UHII_{\mathrm{NO}} > 0$. Black dots refer to HW days exhibiting a peak in UHI averaged for each city.

after the peaks, we also notice that urban temperature begins to grow before the rural, even a few days before the HW development, and then needs more days to stabilise around the climatological mean. We reproduced these curves modifying the HW temporal definition, extending the three days threshold to four and five days. The asymmetric behaviour of UHI was confirmed, so results were qualitatively independent from the methodology. To facilitate the comparison with [29], we also computed the coefficients of the linear regression between $\widetilde{T_U}$ and $\widetilde{T_R}$. Contrarily to [29], we obtained a slope greater than 1 indicating that $\widetilde{T_U}$ increased more than $\widetilde{T_R}$ during warmer conditions, confirming for our analysis the exacerbation of UHI during HW events.

The evolution of standardised mean urban–rural ΔT (figure 5(c)) confirmed the intensification of UHI during HW days, with an evident growth starting before HW onset and reaching its maximum three days after day 0. To quantify the impact of anomalous spikes in temperature values, we conducted the test through moving average described in section 2.6 Even with these modifications, the results demonstrated a similar behaviour as that in figure 5(c), describing a growth in UHI a few days before the HW onset. This asynchronicity between the evolution of the HW and its imprint on the UHI is also retrieved in [14], where maximum UHI occurs before or during the first few days of extreme warm weather, and they use it to prove the absence of temporal correlation between UHI and HWs. However, in our case figure 5(d) allows to put this result in a different context, representing the standardised mean large scale T_{AN} during HW periods. We notice that the raise of ΔT begins simultaneously with the increase in T_{AN}, almost a week before the HW onset. During the first days of HW, when the maximum values of temperature anomaly are reached, also the UHI ΔT experiences an enhancement.

Figure 6 shows a binned scatter plot between large scale T_{AN} and nighttime urban–rural ΔT including all data during both NO and HW days for the 32 cities with $UHII_{\mathrm{NO}} > 0$. The black dots concern days exhibiting the peak of UHI averaged for each city. An increasing trend of ΔT with growing temperature is noticeable, verifying that UHI effect was exacerbated depending on temperature intensity. The black dots revealed that the UHI peaks of $\approx 2\,^\circ$C lie in a range around $T_{\mathrm{AN}} = 4\,^\circ$C, but the highest values of UHI were found for lower values of T_{AN} (about $0\,^\circ$C). This indicates that the behaviour of UHI is partially linked not only to temperature magnitude, but also to the duration of extreme heat conditions. In fact the greatest ΔT regard even NO conditions, events not sufficiently hot or prolonged to be considered HWs. Moreover, we can observe an almost symmetrical behaviour of UHI minima and maxima at $T_{\mathrm{AN}} = -10\,^\circ$C and $0\,^\circ$C.

4. Conclusion

This study investigated the relationship between HW and UHI. To this end, the daily maximum and minimum temperature records (for diurnal and nocturnal UHI, respectively) measured by meteorological stations in 37 European cities were investigated by distinguishing HW days from non-HW days during the summers from 2000 to 2019. We adopted a methodology that allows to select appropriate urban and rural stations, considering different characteristics of the station site such as altitude, distance from the city centre and land cover.

We quantified the UHI magnitude with the composite UHI index (UHII) that is designed to reduce the role of site-specific variability. A HW was defined in this study as a persistent large-scale temperature anomaly diagnosed in reanalysis data.

We found that for the majority of examined cities the nocturnal UHII features a positive climatological mean that increases during HWs on average by 0.7 °C. These cities also showed an increment in the percentage of days with positive UHII. The analysis of the temporal evolution of UHII during HW periods highlighted that the intensification of the UHII is explained by a larger and more persistent increase of urban temperature with respect to rural during a HWs. The intensification peaks at about 1.3 °C, three days after the HW onset, but notably the increment of urban–rural temperature difference starts to strengthen even one week before the HW peaks, making the UHI signal a *de facto* precursor of HW events. The analysis of the relationship between large-scale temperature anomalies and UHII revealed a smooth and continuous relationship between large scale temperatures and UHII, but a large variability. The lack of a threshold behaviour in this relationship suggested that large-scale temperature variability can affect UHI at local scale not only during extreme events. This result can be informative for studies that investigate the relationship between UHI and global warming.

The statistical analysis of temperature data in a large ensemble of cities with remarkably heterogeneous characteristics described in this study is inadequate to shed light on details of physical mechanisms regulating the UHI-HW interaction and of drivers at play. However, it can provide valuable information in the effort to conceptualise the UHI-HW relationship and its multi-scale nature. Indeed, being able to detect features of the UHI-HW synergy that are common to many cities can provide guidance to develop simple models on how synoptic meteorological conditions affect the UHI, and can foster the development of simplified large-scale methodologies for the assessment of health-related threats of temperature extremes in urban environment. For instance, results in figures 5 and 6 suggest that, while UHII and large scale temperature are strongly correlated (figure 6), HWs phenomena should exhibit synoptic conditions that favour a strong UHI even when the large-scale temperature anomaly of the HW is not mature (figure 5(c)). This is an indication to further explore the UHI-HW relationship focusing also on the synoptic scale circulation before the HW has reached a mature stage. Along these lines, future studies could look for meteorological variables other than temperature that exhibit a sharp collapse like the one found in figure 5(c). Moreover, the temporal asymmetry found in the UHI-HW lead-lag relationship can *per se* provide guidance in prospective development of early warning systems.

This study provides observational evidence of the synergistic interaction between the nighttime UHI and HWs by applying for the first time a homogeneous methodology to *in situ* observations in a large cluster of European cities. Overall the results for data presented in this work support the conclusion that the UHI exhibits an exacerbation during HW events in the majorities of European cities, and this is becoming an increasingly dominant paradigm in scientific literature (see [16, 26, 28]). Our results suggest that the conclusion reached by [29], who with a similar methodology found a reduction of the UHI during hot days in many US cities, do not hold for the majority of European cities analysed in our study, which is in accordance with recent existing literature on case studies (e.g. [31–33]). Nonetheless, the emergence in our study of predominantly negative UHII values in a small cluster of cities may deserve attention in future investigations.

Data availability statement

All data that support the findings of this study are included within the article (and any supplementary files).

Acknowledgment

This research was funded by the OPERANDUM project. This project has received funding from the European Union's Horizon 2020 research and innovation program under grant agreement No. 776848. The authors thank ECA&D, WMO and Copernicus for providing open access data. The authors acknowledge the use of computational resources from the parallel computing cluster of the Open Physics Hub (https://site.unibo.it/openphysicshub/en) at the Physics and Astronomy Department in Bologna.

ORCID iDs

Marco Possega https://orcid.org/0000-0002-0781-7051
Leonardo Aragão https://orcid.org/0000-0003-2843-505X
Paolo Ruggieri https://orcid.org/0000-0003-1996-7206
Marco Antonio Santo https://orcid.org/0000-0003-4189-2714
Silvana Di Sabatino https://orcid.org/0000-0003-2716-9247

References

[1] De Bono A, Peduzzi P, Kluser S and Giuliani G 2004 Impacts of summer 2003 heat wave in Europe
[2] Guha-Sapir D, Below R and Hoyois P. 2016 EM-DAT: the CRED/OFDA international disaster database

[3] Barriopedro D, Fischer E M, Luterbacher J, Trigo R M and García-Herrera R 2011 The hot summer of 2010: redrawing the temperature record map of Europe *Science* **332** 220–4
[4] Masson-Delmotte V *et al* 2021 IPCC, 2021: Summary for Policymakers. *Climate Change 2021: The Physical Science Basis. Contribution of Working Group I to the Sixth Assessment Report of the Intergovernmental Panel on Climate Change*
[5] Guerreiro S B, Dawson R J, Kilsby C, Lewis E and Ford A 2018 Future heat-waves, droughts and floods in 571 European cities *Environ. Res. Lett.* **13** 034009
[6] Fischer E M and Schär Ç 2010 Consistent geographical patterns of changes in high-impact european heatwaves *Nat. Geosci.* **3** 398–403
[7] Perkins-Kirkpatrick S E and Gibson P B 2017 Changes in regional heatwave characteristics as a function of increasing global temperature *Sci. Rep.* **7** 1–12
[8] Oke T R 1982 The energetic basis of the urban heat island *Q. J. R. Meteorol. Soc.* **108** 1–24
[9] Oke T R, Mills G, Christen A and Voogt J A 2017 *Urban Climates* (Cambridge: Cambridge University Press)
[10] Wang Y, Di Sabatino S, Martilli A, Li Y, Wong M S, Gutiérrez E and Chan P W 2017 Impact of land surface heterogeneity on urban heat island circulation and sea-land breeze circulation in Hong Kong *J. Geophys. Res. Atmos.* **122** 4332–52
[11] An N, Dou J, González-Cruz J E, Bornstein R D, Miao S and Li L 2020 An observational case study of synergies between an intense heat wave and the urban heat island in Beijing *J. Appl. Meteorol. and Climatol.* **59** 605–20
[12] He B-J, Wang J, Zhu J and Qi J 2022 Beating the urban heat: situation, background, impacts and the way forward in China *Renew. Sustain. Energy Rev.* **161** 112350
[13] Jiang L, Chen Y D, Li J and Liu C 2022 Amplification of soil moisture deficit and high temperature in a drought-heatwave co-occurrence in southwestern China *Nat. Hazards* **111** 641–60
[14] Richard Y, Pohl B, Rega M, Pergaud J, Thevenin T, Emery J, Dudek J, Vairet T, Zito S and Chateau-Smith C 2021. Is urban heat island intensity higher during hot spells and heat waves (Dijon, France, 2014–2019)? *Urban Clim.* **35** 100747
[15] Kumar R and Mishra V 2019 Decline in surface urban heat island intensity in India during heatwaves *Environ. Res. Commun.* **1** 031001
[16] Zhao L, Oppenheimer M, Zhu Q, Baldwin J W, Ebi K L, Bou-Zeid E, Guan K and Liu X 2018 Interactions between urban heat islands and heat waves *Environ. res. lett.* **13** 034003
[17] Ramamurthy P and Bou-Zeid E 2017 Heatwaves and urban heat islands: a comparative analysis of multiple cities *J. Geophys. Res. Atmos.* **122** 168–78
[18] Li D and Bou-Zeid E 2013 Synergistic interactions between urban heat islands and heat waves: the impact in cities is larger than the sum of its parts *J. Appl. Meteorol. Climatol.* **52** 2051–64
[19] Chew L W, Liu X, Li X and Norford L K 2021 Interaction between heat wave and urban heat island: a case study in a tropical coastal city, singapore *Atmos. Res.* **247** 105134
[20] Kunkel K E, Changnon S A, Reinke B C and Arritt R W 1996 The July 1995 heat wave in the midwest: a climatic perspective and critical weather factors *Bull. Am. Meteorol. Soc.* **77** 1507–18
[21] Schatz J and Kucharik C J 2015 Urban climate effects on extreme temperatures in Madison, Wisconsin, USA *Environmen. Res. Lett.* **10** 094024
[22] Rizvi S H, Alam K and Iqbal M J 2019 Spatio-temporal variations in urban heat island and its interaction with heat wave *J. Atmos. Sol. Terr. Phys.* **185** 50–57
[23] He X, Wang J, Feng J, Yan Z, Miao S, Zhang Y and Xia J 2020 Observational and modeling study of interactions between urban heat island and heatwave in Beijing *J. Clean. Prod.* **247** 119169
[24] Katavoutas G and Founda D 2019 Response of urban heat stress to heat waves in Athens 1960–2017 *Atmosphere* **10** 483
[25] He B-J, Wang J, Liu H and Ulpiani G 2021 Localized synergies between heat waves and urban heat islands: implications on human thermal comfort and urban heat management *Environ. Res.* **193** 110584
[26] Miao S *et al* 2022 Heat wave-induced augmentation of surface urban heat islands strongly regulated by rural background *Sustainable Cities and Society* **82** 103874
[27] Oliveira A, Lopes A, Correia E, Niza S and Soares A 2021 Heatwaves and summer urban heat islands: a daily cycle approach to unveil the urban thermal signal changes in lisbon, Portugal *Atmosphere* **12** 292
[28] Kong J, Zhao Y, Carmeliet J and Lei C 2021 Urban heat island and its interaction with heatwaves: a review of studies on mesoscale *Sustainability* **13** 10923
[29] Scott A A, Waugh D W and Zaitchik B F 2018 Reduced urban heat island intensity under warmer conditions *Environmen. Res. Lett.* **13** 064003
[30] Antipova A 2018 Urban environment: the differences between the city in Europe and the United States *Urban Environment, Travel Behavior, Health and Resident Satisfaction* (Berlin: Springer) pp 35–117
[31] Founda D and Santamouris M 2017 Synergies between urban heat island and heat waves in Athens (Greece), during an extremely hot summer (2012) *Sci. Rep.* **7** 1–11
[32] Nicholson A 2020 Analysis of the diurnal cycle of air temperature between rural Berkshire and the university of reading: possible role of the urban heat island *Weather* **75** 235–41
[33] Unger J, Skarbit N, Kovács A and Gal T 2020 Comparison of regional and urban outdoor thermal stress conditions in heatwave and normal summer periods: a case study *Urban Clim.* **32** 100619
[34] Wong K V, Paddon A and Jimenez A 2013 Review of world urban heat islands: many linked to increased mortality *J. Energy Resour. Technol.* **135** 022101
[35] Klein Tank A M G *et al* 2002 Daily dataset of 20th-century surface air temperature and precipitation series for the European climate assessment *Int. J. Climatol* **22** 1441–53
[36] Klok E J and Klein Tank A M G 2009 Updated and extended European dataset of daily climate observations *Int J. Clim.* **29** 1182–91
[37] Smith A, Lott N and Vose R 2011 The integrated surface database: recent developments and partnerships *Bull. Am. Meteorol. Soc.* **92** 704–8
[38] Rasilla D, Allende F, Martilli A and Fernàndez F 2019 Heat waves and human well-being in Madrid (Spain) *Atmosphere* **10** 288
[39] Stefanon M, D'Andrea F and Drobinski P 2012 Heatwave classification over Europe and the mediterranean region *Environ. Res. Lett.* **7** 014023
[40] Hooyberghs H, Berckmans J, Lauwaet D, Lefebre F and De Ridder K 2019 Climate variables for cities in Europe from 2008 to 2017, version 1.0, Copernicus Climate Change Service (C3S) Climate Data Store (CDS) (Accessed 4 November 2022)
[41] EEA Corine Land Cover (CLC) 2018 Version 20b2, 2018 (available at: https://land.copernicus.eu/pan-european/corine-lan d-cover/clc2018) (Accessed 4 November 2022)
[42] Hersbach H *et al* 2018 ERA5 hourly data on single levels from 1959 to present. Copernicus climate change service (C3S) climate data store (CDS), (Accessed 4 November 2022)
[43] Rousi E, Kornhuber K, Beobide-Arsuaga G, Luo F and Coumou D 2022 Accelerated western European heatwave trends linked to more-persistent double jets over Eurasia *Nat. commun.* **13** 1–11
[44] Di Napoli C, Barnard C, Prudhomme C, Cloke H L and Pappenberger F 2021 ERA5-HEAT: A global gridded historical dataset of human thermal comfort indices from climate reanalysis *Geosci. Data J.* **8** 2–10
[45] Berckmans J, Lefebre F, Hooyberghs H, De Ridder K, de'Donato F, Ducheyne E, Marsboom C, Páldy A, Adamonyte D, Voitonis E 2021 Heat wave days for European countries derived from ERA5 reanalysis

(available at: https://cds.climate.copernicus.eu/cdsapp#!/software/app-health-heat-waves-current-climate?tab=app)
[46] European Statistics (Eurostat) (available at: https://ec.europa.eu/eurostat/data/database) accessed 4 November 2022)
[47] Wolfram Research, Inc. Wolfram—Alpha Knowledgebase 2022 (Champaign, IL)
[48] EEA Copernicus land monitoring service-urban atlas 2017 (available at: https://www.eea.europa.eu/data-and-maps/data/copernicus-land-monitoring-serviceurban-atlas.) (Accessed 4 November 2022)
[49] Li K, Chen Y, Wang M and Gong A 2019 Spatial-temporal variations of surface urban heat island intensity induced by different definitions of rural extents in China *Sci. Tot. Environ.* **669** 229–47
[50] Zhang P, Imhoff M L, Wolfe R E and Bounoua L 2010 Characterizing urban heat islands of global settlements using MODIS and nighttime lights products *Can. J. Remote Sens.* **36** 185–96
[51] Martin-Vide J, Sarricolea P and Moreno-García M C 2015 On the definition of urban heat island intensity: the 'rural' reference *Frontiers Earth Sci.* **3** 24
[52] Ngarambe J, Nganyiyimana J, Kim I, Santamouris M and Yun G Y 2020 Synergies between urban heat island and heat waves in Seoul: the role of wind speed and land use characteristics *PLoS One* **15** e0243571
[53] Schumacher U 2021 The urban mask layer as reference geometry for spatial planning: moving from German to European geodata *KN-Journal of Cartography and Geographic Information* **71** 83–95
[54] Berckmans J, Lefebre F, Hooyberghs H, De Ridder K, de'Donato F, Ducheyne E, Marsboom C, Páldy A, Adamonyte D, Voitonis E 2020 Demo web-application URBAN.1 - C3S_422_Lot2_VITO - European Health
[55] Herbel I, Croitoru A-E, Rus A V, Roşca C F, Harpa G V, Ciupertea A-F and Rus I 2018 The impact of heat waves on surface urban heat island and local economy in Cluj-napoca city, romania *Theor. Appl. Climatol.* **133** 681–95
[56] Pyrgou A, Hadjinicolaou P and Santamouris M 2020 Urban-rural moisture contrast: regulator of the urban heat island and heatwaves' synergy over a Mediterranean city *Environmen. Res.* **182** 109102
[57] Basara J B, Hall J P K, Schroeder A J, Illston B G and Nemunaitis K L 2008 Diurnal cycle of the Oklahoma City urban heat island *J. Geophys. Res. Atmos.* **113** (D20)
[58] Basara J B, Illston B G and Crawford K C 2010 The impact of the urban heat island during an intense heat wave in Oklahoma city *Adv. Meteorol.* **2010** 1–10
[59] Oke T R 2002 *Boundary Layer Climates* (London: Routledge)
[60] Welch B L 1947 The generalization of Student's problem when several different population variances are involved *Biometrika* **34** 28–35
[61] Ruxton G D 05 2006 The unequal variance t-test is an underused alternative to student's t-test and the Mann–Whitney u test *Behav. Ecology* **17** 688–90
[62] Wilks D S 2011 *Statistical Methods in the Atmospheric Sciences* vol 100 (New York: Academic)
[63] Oliver E C J *et al* 2019 Projected marine heatwaves in the 21st century and the potential for ecological impact *Front. Mar. Sci.* **6** 734